Journal of Sustainable Metallurgy (2021) 7:1–14
https://doi.org/10.1007/s40831-020-00318-y

RESEARCH ARTICLE

Slag Chemistry and Behavior of Nickel and Tin in Black Copper Smelting with Alumina and Magnesia-Containing Slags

Anna Dańczak[1] · Lassi Klemettinen[1] · Hugh O'Brien[2] · Pekka Taskinen[1] · Daniel Lindberg[1] · Ari Jokilaakso[1]

Received: 5 August 2020 / Accepted: 23 November 2020 / Published online: 21 December 2020

Abstract

The global amount of waste electrical and electronic equipment (WEEE) is growing fast. Non-ferrous metals represent a large portion of this waste, and they can be potentially recovered via black copper smelting. Alumina and magnesia, originating from the e-waste or fluxes, can be present in the feed of a secondary copper smelter in varying concentrations. Our study focuses on the impact of MgO on the slag chemistry of high-alumina iron silicate slags. The distributions of tin and nickel as minor elements were also investigated and compared with literature data. The equilibrium study was performed at 1300 °C in reducing conditions. Three different slag mixtures with 0, 3, and 6 wt% MgO were used in the study. The MgO addition significantly reduced the solubility of alumina in the slag and changed the primary spinel phase composition. The combined effects of increasing MgO and decreasing Al_2O_3 concentration in the slag regarding the distribution of tin were noticeable, i.e., its deportment to metal phase increased, but for nickel the effect was negligible. Theoretical calculations were performed for estimating the isolated effect of MgO on the distributions and they confirmed the beneficial effect on the behavior of tin but showed no impact for nickel.

The contributing editor for this article was Yongxiang Yang.

Supplementary information The online version of this article (https://doi.org/10.1007/s40831-020-00318-y) contains supplementary material, which is available to authorized users.

✉ Anna Dańczak
anna.danczak@aalto.fi

Lassi Klemettinen
lassi.klemettinen@aalto.fi

Hugh O'Brien
hugh.obrien@gtk.fi

Pekka Taskinen
pekka.taskinen@aalto.fi

Daniel Lindberg
daniel.k.lindberg@aalto.fi

Ari Jokilaakso
ari.jokilaakso@aalto.fi

[1] Department of Chemical and Metallurgical Engineering, School of Chemical Engineering, Aalto University, Kemistintie 1, P.O. Box 16100, 00076 Aalto, Finland

[2] Geological Survey of Finland, Vuorimiehentie 2, 02150 Espoo, Finland

Graphical Abstract

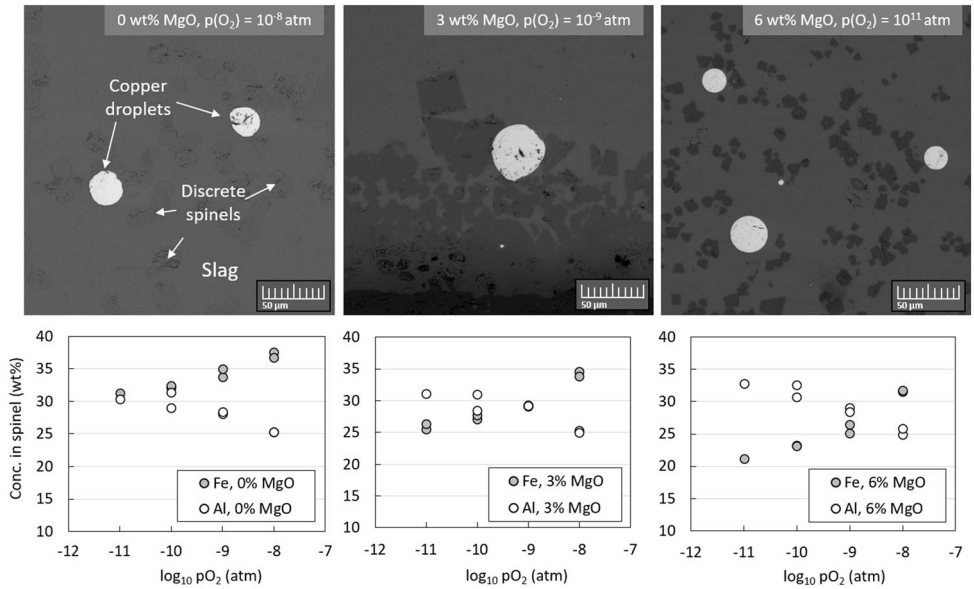

Keywords Thermodynamics · Recycling · Circular economy · e-waste

Introduction

The production of EEE (Electrical and Electronic Equipment) has grown rapidly in recent years, resulting in increased generation of waste as the equipment reaches end-of-life. The quantity of this waste, referred to as WEEE (Waste Electrical and Electronic Equipment), is estimated to reach approximately 52 million tonnes by 2021 [1]. WEEE consists of a varied range of materials; iron and steel account for almost half and plastics represent about 21% of the overall weight of WEEE. The third largest component by weight, about 13% of WEEE, is non-ferrous metals [2]. WEEE is a rich source of critical raw materials (CRMs), which are widely used in emerging technologies [3]. Securing access to CRMs is one of the biggest challenges for the modern metallurgical industry and therefore, the CRM recovery technologies from WEEE are of very high interest.

An effective route to recover some non-ferrous metals, such as copper, as well as precious metals from WEEE is pyrometallurgy [4]. Pyrometallurgical methods for industrial WEEE recycling have been described in many review articles and books [5, 6]. One of the possible routes is a smelting process where WEEE is injected into a high temperature furnace and the recycling process is integrated into the base metal production chain. The base metal (copper, lead, or nickel) acts as a collector for valuable metals such as gold, silver, platinum group metals (PGMs) [4], and some other metals classified as CRMs [3].

Ghodrat et al. [7] conducted an analysis of electronic waste recycling through black copper smelting and confirmed that this route has considerable potential both in its technical and economic efficiency. It consists of subsequent reducing and oxidizing steps where typically slag in the oxidizing step is recirculated back to the reductive step. However, the elements as well as their concentrations vary significantly between WEEE and primary ores and conventional scrap [8]. The presence of many different trace and major elements can influence each other's behavior and consequently their recoveries in ways not thoroughly understood yet. Therefore, developing and designing optimal processes and operating parameters for different smelters using secondary raw materials in their feed is one of the today's greatest challenges for the metal industries [9].

WEEE contains from 1 to 11 wt% of aluminum [10, 11], making it a common impurity in black copper smelting. Additionally, copper slags usually contain about 1 to 10 wt% of CaO and MgO, designedly or otherwise [10]. The presence of these oxides in the molten slag changes slag basicity and affects the physical properties, viscosity, and melting temperature of the slags [12]. Therefore, it enhances the stabilities of solid primary phases. This affects the slag saturation boundaries and elemental solubilities [10]. There are still gaps in knowledge on the effects of different additives on the slag properties and on the deportment of different

trace elements in the secondary copper processing. Fundamental experimental data are required for improved process development, evaluation, and optimization.

The impact of CaO and MgO additions on the viscosity of iron silicate slag was measured by Kowalczyk et al. [13]. The results showed that as long as the slag remains fully liquid, the additions of MgO and CaO slightly decrease the slag viscosity. However, when the slags reached MgO and/or CaO saturation, their viscosity increased sharply.

Elliot et al. [14] investigated the effects of CaO, Al_2O_3, and MgO additions on copper solubility in silica-saturated fayalite slag. The results confirmed that copper dissolves as $CuO_{0.5}$ in the slag and indicated that the copper solubility decreased significantly with an increasing amount of CaO in the slag mixture and decreased slightly with the presence of Al_2O_3 and MgO. The significant impact of CaO concentration on copper solubility in FeO_x–SiO_2 slags has been confirmed by further studies and presented also in thermodynamic databases [15].

Kim and Sohn [10] investigated the impacts of CaO, Al_2O_3, and MgO additions in silica-saturated FeO_x–SiO_2 slags on the behavior of trace elements Bi, Sb, and As. They indicated that small concentrations (about 4.4 wt%) of CaO, Al_2O_3, and MgO in the slag increased the distribution coefficients of Bi and Sb between metallic copper and slag, whereas higher additive concentrations (about 8 to 11 wt%) had a smaller effect on the Bi and Sb distributions. The study did not indicate a significant effect of CaO, Al_2O_3, and MgO on the partition of As [10].

Phase equilibria between copper alloy and iron silicate slags with small additions of CaO, Al_2O_3, and MgO was investigated by Henao et al. [16, 17]. The primary phase fields of tridymite, spinel, olivine, and clinopyroxene were identified and spinel and tridymite liquidus contours were constructed.

Recently, Hasan et al. [18] studied the structure of ferrous calcium-silicate slags with MgO addition using Fourier-transform infrared (FTIR) spectrometry. They showed that the overall degree of polymerization (DOP) of the silicate network and the average number of bridging oxygen (BO) decreased with increasing both the Fe/SiO_2 ratio and basicity (defined as CaO/SiO_2 ratio).

Avarmaa et al. [19] studied the partition behavior of tin as a trace element between metallic copper alloys and different iron silicate-based slags. They also conducted a thorough review on the earlier studies related to the behavior of tin in copper smelting conditions. In general, tin can be recovered in the copper alloy in reducing conditions, but in an oxidizing atmosphere it is volatilized or deported into the slag. In this study, tin is not present as a trace element, as its initial concentration in the alloy was 5%. The distribution behavior of nickel in secondary copper smelting conditions with alumina-containing slags has been studied by Klemettinen et al. [20], who also reviewed the earlier-related literature.

In our previous study [21], the suitability of black copper smelting process for recycling of battery metals lithium, cobalt, manganese, and lanthanum was investigated. The oxygen partial pressure range between 10^{-11} and 10^{-8} atm was used in the experiments to simulate different unit processes in copper smelting, especially the ones operating in reducing conditions (e.g., slag cleaning process and reduction step in Ausmelt type of furnace). The behavior of these battery metals in the same experimental conditions as in this study is described in detail. In comparison to our previous work, the current study focuses on investigating the effect of MgO on the slag chemistry of high-alumina iron silicate slags. Additionally, the behavior of tin and nickel as minor elements, originating from WEEE, in black copper smelting conditions was investigated.

Experimental

Slag (oxide) and copper (metal alloy) mixtures were prepared from pure, commercially available powders. The slags represent mixtures of Al_2O_3 (99.99%, Sigma-Aldrich), Fe_2O_3 (99.999%, Alfa Aesar), SiO_2 (99.995%, Alfa Aesar), and MgO (99.95%, Alfa Aesar). The slag mixtures had an initial Fe/SiO_2 ratio of 1.3 and an Al_2O_3 concentration of 15 wt%. Three slag mixtures, with 0, 3, and 6 wt% MgO, were prepared in order to investigate the effects of MgO on the equilibrium system. Additionally, trace elements La, Mn, and Li were added to the slag mixtures in the form of La_2O_3 (99.9%, Alfa Aesar), MnO (99.99%, Alfa Aesar), and Li_2CO_3 (99.998%, Alfa Aesar), respectively. The three starting slag mixtures contained 1 wt% of La, Mn, and Li each. The copper alloy was mixed from Cu (Alfa Aesar, 99.9%) with 5 wt% Sn (99.85%, Alfa Aesar), 2 wt% Ni (99.996%, Alfa Aesar), and 1 wt% Co (99.99%, Koch-Light Laboratories Ltd). This article focuses on the slag chemistry and behavior of nickel and tin. The behaviors of Li, Co, Mn, and La were described in our previous study [21].

Equilibration of the samples took place at 1300 °C in a vertical laboratory furnace in the oxygen partial pressure (pO_2) range from 10^{-11} to 10^{-8} atm. The furnace arrangement and details were presented in a previous study of Klemettinen et al. [22]. The experimental temperature was controlled with a calibrated S-type Pt/Pt10Rh thermocouple (Johnson-Matthey, UK). The temperature uncertainty was ± 3 °C. 200 mg of both slag mixture and copper alloy were weighed in an alumina crucible (Frialit AL 23, 8/15 mm ID/H, Friatec AG, Germany). The crucible was held in a Pt-wire basket, hooked with a platinum–rhodium wire, and pulled up to the hot zone of the furnace. The gas atmosphere in the experimental furnace was a mixture of

CO_2 (99.9993%, Linde-AGA, Finland) and CO (99.97%, Linde-AGA, Finland). These gases were introduced to the furnace through mass flow controllers (Aalborg, DFC26, USA) held at room temperature (~ 20 °C). The gas flow was introduced to the work tube, sealed from the outside atmosphere, 30 min before pulling the sample into the hot zone to ensure complete flushing and removal of laboratory air. The desired oxygen partial pressures were created using different CO_2/CO ratios calculated at the experimental temperature (1300 °C) with MTDATA software and the SGTE pure substances database [23]. The total gas flow rate was 300 ml/min. The flow rates of CO_2 and CO for obtaining the desired oxygen partial pressures have been presented earlier [21]. The furnace work tube was flushed with Ar (99.999%, Linde-AGA, Finland) after every experiment in order to remove the CO_2–CO mixture.

The equilibrated samples were quenched to solid state very rapidly, in 2–3s. Before quenching, a plastic quenching vessel filled with ice–water mixture was placed under the furnace work tube so that approximately 5 cm of the bottom part of the tube was immersed in the ice–water mixture. The bottom of the furnace work tube was unplugged while being covered with the ice–water mixture, thus preventing air from entering the tube. The time between unplugging the work tube and dropping the sample to the quenching vessel was only a few seconds. The quenched samples were cut in half, mounted in epoxy (Struers, Denmark), and polished using traditional dry metallographic methods. After polishing, the samples were carbon-coated to ensure sufficient electrical conductivity for compositional analyses from the cross sections.

The equilibration time necessary for reaching uniform chemical compositions of all phases in the copper alloy—FeO_x–SiO_2–Al_2O_3–MgO slag—iron-alumina spinel system was investigated in pre-experiments conducted at 1300 °C and oxygen partial pressure $p(O_2) = 10^{-10}$ atm. Annealing times of 4, 8, 16, 24, and 48 h were used. The microstructures of all samples were analyzed using a Mira3 SEM (Scanning Electron Microscope, Tescan, Czech Republic) and the elemental compositions of the samples from the time series experiments were determined with an UltraDry Silicon Drift EDS (Energy Dispersive Spectrometer, Thermo Fisher Scientific, USA). Thermo-Scientific NSS Spectral Imaging software with Proza ZAF matrix correction [24] was used for the quantitative investigations. An acceleration voltage of 15 kV and a beam current of 11 nA were applied during the analyses. The concentrations of Si, Al, and Mg in the slag phase as a function of time, with standard deviations, are presented in Fig. 1. Based on the results, 24 h was selected to ensure equilibrium for every experiment. Duplicate experiments were conducted for reliability, and every experiment is presented with its own symbol in the graphs.

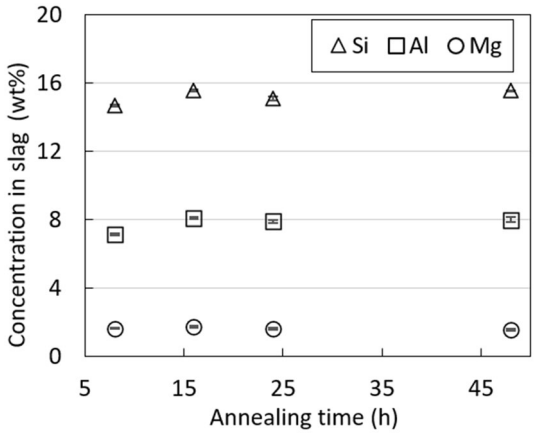

Fig. 1 Concentrations of silicon, aluminum, and magnesium in the slag as a function of time in $p(O_2) = 10^{-10}$ atm. One-standard-deviation error bars for the data plots are visible within the symbols

The chemical compositions of the 24-h equilibrium experiments were analyzed with EPMA (Electron Probe MicroAnalysis) and LA-ICP-MS (Laser Ablation–Inductively Coupled Plasma–Mass Spectrometry). An SX-100 Microprobe (Cameca SAS, France) with 20 kV accelerating voltage and 60 nA beam current was used. A minimum of 8 (slag and alloy) or 6 (spinel) points were analyzed from each sample. The analyzed X-ray lines, standards, and obtained detection limits are presented in Table 1. The elemental compositions of metal, slag, and spinel phases have been collected in Supplementary Tables S-1–S-3 (refer to Supplementary Information).

Both slag and copper alloy (from one experimental series) were also analyzed with LA-ICP-MS for accurate measurement of trace element concentrations. The slag phase was analyzed with 65 µm laser spot size, firing frequency of 10 Hz, 4 ns laser pulses, and a fluence of 2.5 J/cm^2 on the sample surface. This article utilizes the LA-ICP-MS results only for the slag phase at low oxygen partial pressures; the analysis settings for the metal phase, as well as the details of the equipment, have been presented previously [21]. The time-resolved analysis signals were collected over 400 laser pulses and data reduction was conducted using Glitter software [25]. The standards used and detection limits obtained are summarized in Table 1.

Results and Discussion

Microstructure

Sample microstructure was relatively similar for all samples regardless of the slag composition. A typical microstructure, presented in Fig. 2a, consisted of metal alloy, glassy slag, spinel (rim on the interface of slag and crucible, as

Table 1 Standards used and detection limits obtained in EPMA and LA-ICP-MS analyses

EPMA								
	O	Si	Al	Mg	Fe	Cu	Ni	Sn
Analyzed X-ray line	Kα	Kα	Kα	Kα	Kα	Kα	Kα	Lα
Standard	Hematite	Quartz	Almandine	Diopside	Hematite	Cu	Pentlandite	Sn
Det. limit (ppmw)								
Cu alloy	451	149	133	175	77	348	268	153
Slag	1088	203	203	91	199	278	94	146
Spinel	1082	81	216	91	204	113	111	145

LA-ICP-MS		
	Ni	Sn
External standard for slag	NIST610 [26]	
Internal standard for slag	^{29}Si	
Detection limit for slag (ppmw) for the isotope used	^{61}Ni: 0.571	^{118}Sn: 0.013

ppmw parts per million by weight

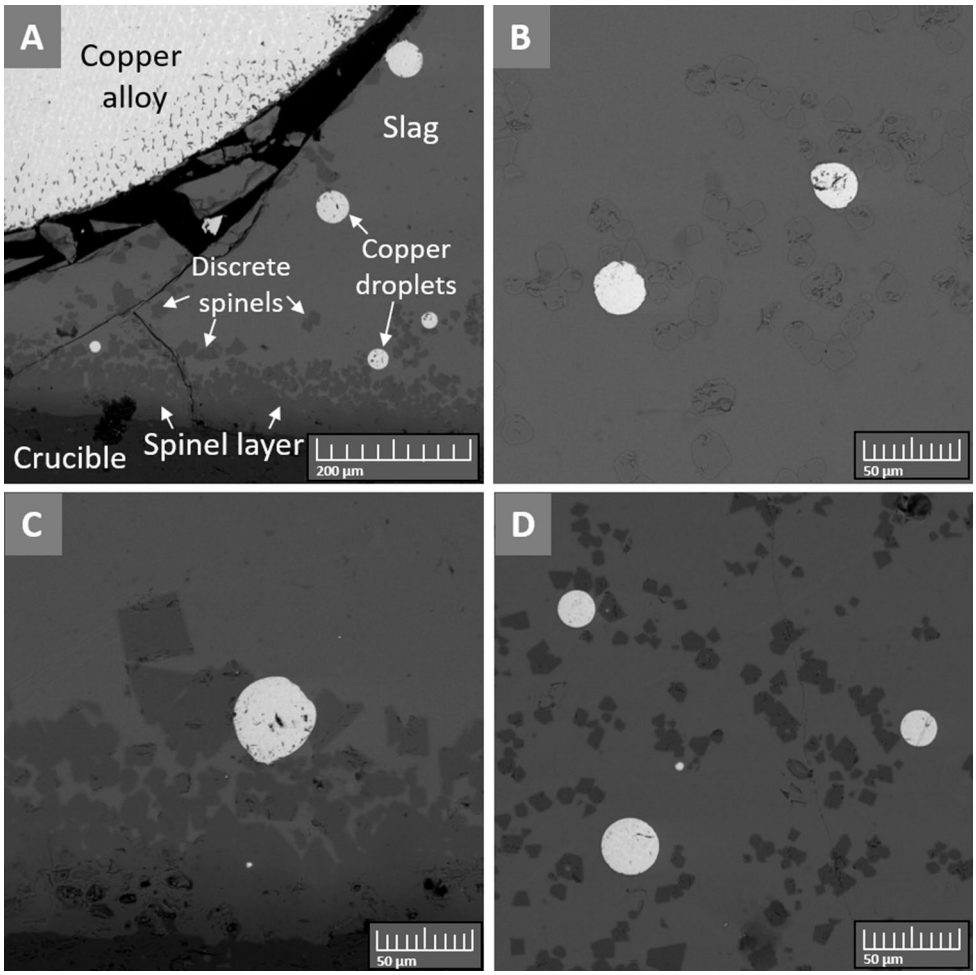

Fig. 2 **a** Typical sample microstructure ($T = 1300$ °C, $p(O_2) = 10^{-10}$ atm, 3 wt% MgO in the slag mixture). **b–d** Discrete spinels within the slag phase in selected samples [**b** $p(O_2) = 10^{-8}$ atm, 0 wt% MgO; **c** $p(O_2) = 10^{-9}$ atm, 3 wt% MgO; **d** $p(O_2) = 10^{-11}$ atm, 6 wt% MgO]

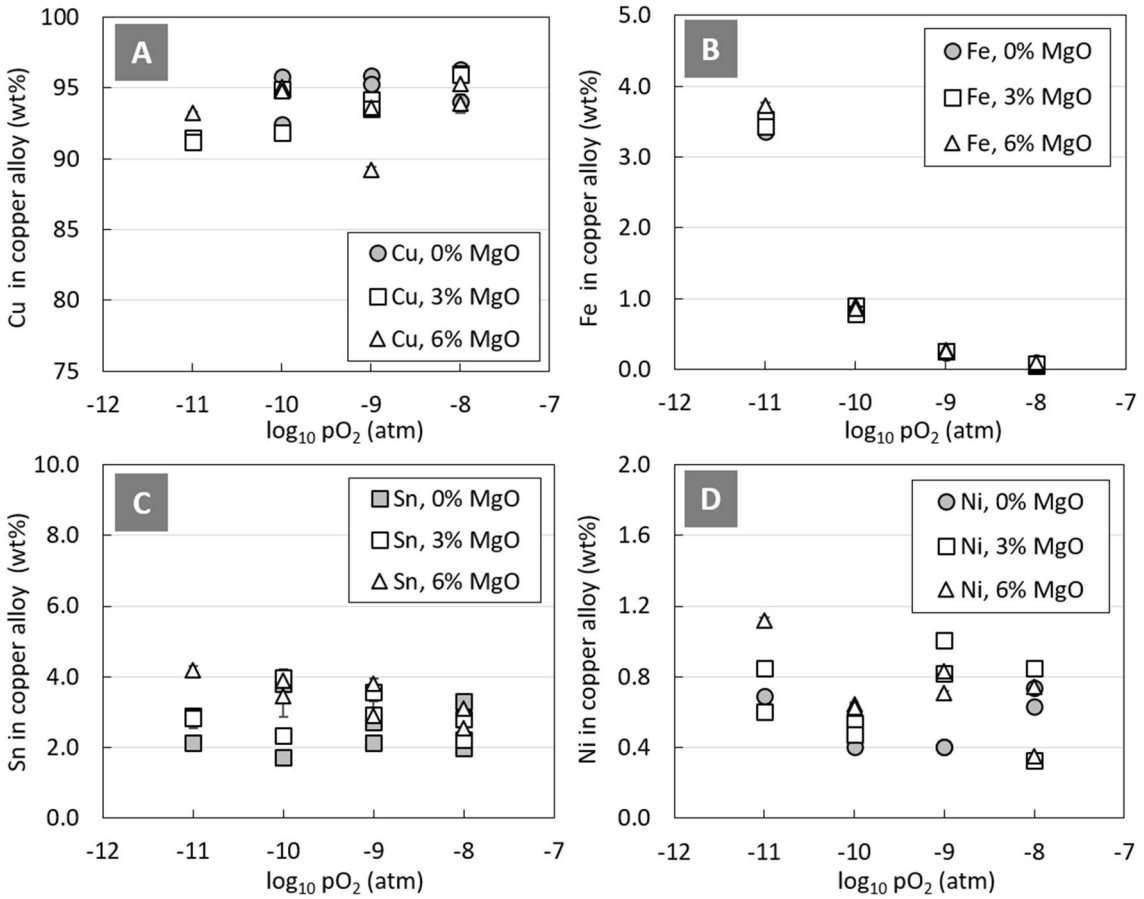

Fig. 3 Copper, iron, tin, and nickel concentrations in copper alloy as a function of oxygen partial pressure. All values are from EPMA. Duplicate experiments are shown with their own respective symbols. One-standard-deviation error bars are also shown, and they are mostly smaller than the symbols

well as individual spinel grains), and the alumina crucible. Figure 2b–d presents details of the slag and spinel phases at different oxygen partial pressures and different MgO concentrations. No evidence of insufficient quenching rate was observed in the slag and spinel phases, as they appeared homogeneous throughout the samples. Tin-rich segregations, possibly formed during quenching, were observed in the larger copper alloy droplets.

In all samples, iron-alumina spinel formed as a dense layer on the interface between the alumina crucible and the slag, resulting in direct iron-alumina spinel saturation and in indirect alumina saturation of the copper-slag system [27]. Small individual spinel grains were also crystallized in all samples, as shown in Fig. 2a–d. The number of spinel grains observed in the slag seemed to increase with the increasing concentration of MgO in the starting slag composition. Similar results have been obtained for CaO-containing slags, as described by Avarmaa et al. [27].

Adhesion of some small and medium-sized copper alloy droplets to individual spinel grains restricted droplet movement, resulting in incomplete phase separation by preventing the droplets from settling fully into the underlying liquid alloy. This phenomenon was indicated in previous studies [28–30]. De Wilde and Bellemans et al. [28, 31–33] have published numerous articles investigating this phenomenon; the origin of the droplets and the effect of slag-spinel composition on the droplet attachment. In those studies, the authors concluded that this phenomenon is determined by the thermodynamic parameters of the systems, i.e., the oxygen partial pressure, the slag composition, and the amount of other metals in the alloy. In our study, the number of entrained copper droplets seemed to increase at higher oxygen partial pressures. According to De Wilde et al. [32], copper droplets only attached to Fe-rich spinels, and not to Al-rich ones. In this work, the droplets were attached to both Fe-rich (higher pO_2) spinel grains (Fig. 2b) and Al-rich (lower pO_2) spinel grains (Fig. 2d). The compositional changes in the spinel as a function of oxygen partial pressure and MgO concentration are discussed in 'Spinel' section.

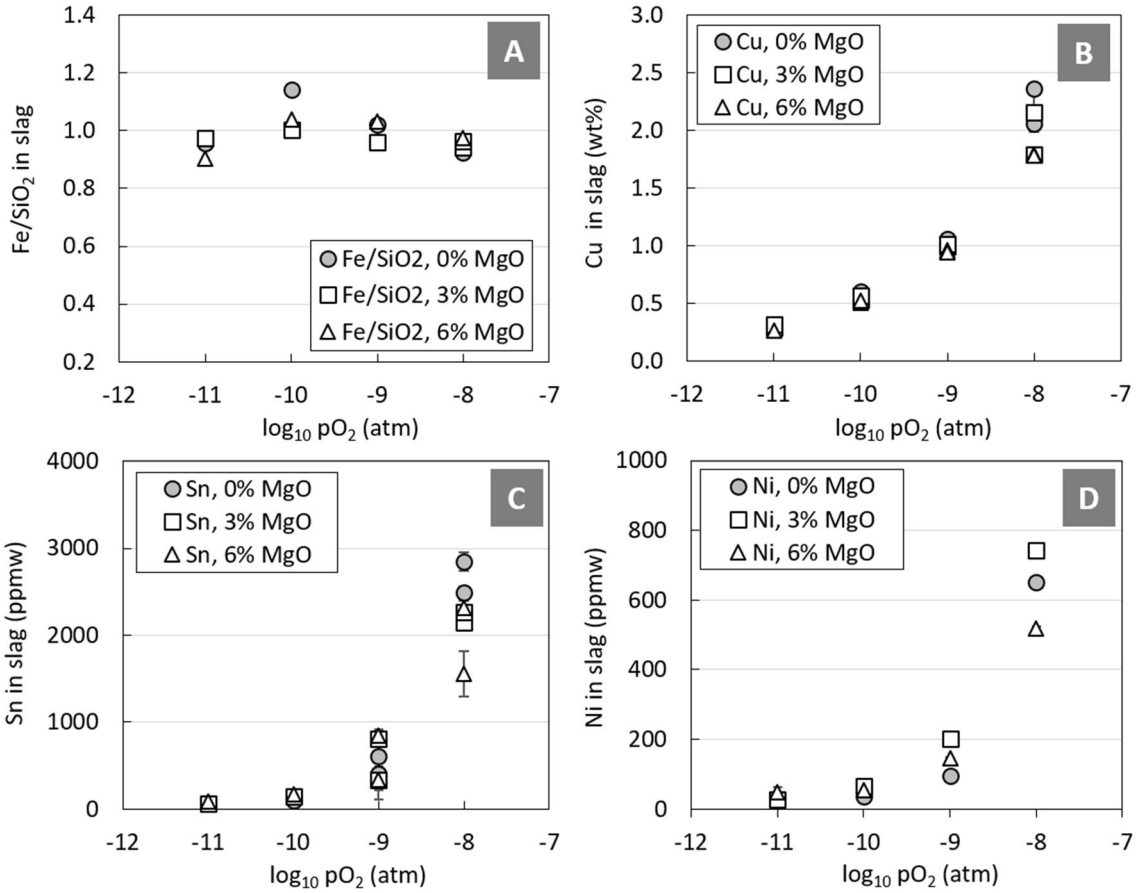

Fig. 4 Fe/SiO_2 ratio and the concentrations of copper, tin, and nickel in the slags as a function of oxygen partial pressure

Phase Compositions

Copper Alloy

Figure 3 shows the changes in copper, iron, tin, and nickel concentrations in the copper alloy as the $p(O_2)$ increases. The copper concentration in the alloy increased with increasing oxygen partial pressure, from approximately 92 to 95 wt%, mostly due to the decreasing iron concentration. The concentrations of nickel and tin in copper alloy varied quite significantly, from 0.35 to 1.1 wt% and from 1.7 to 4.2 wt% for nickel and tin, respectively. This deviation can be attributed to the structure of the metal phase after quenching, as tin-rich segregations were formed in all experimental conditions, regardless of the rapid quenching rate. No clear trends were observed in the investigated $p(O_2)$ range, however, in more oxidizing conditions the concentrations of both nickel and tin in the alloy should decrease drastically [20, 27, 29]. The addition of MgO to the system did not have a clear effect on the equilibrium concentrations of other elements in the copper alloy. The concentration of magnesium in the alloy, in the MgO-containing systems, was between 4 and 7 ppmw with no clear dependency on the amount of MgO added.

Slag

Iron-to-silica ratio is a distinctive parameter of slags and it is typically used as a control variable in industrial processes. Figure 4a shows the Fe/SiO_2 ratio (wt%/wt%) as a function of oxygen partial pressure. The maximum value was reached at $p(O_2) = 10^{-10}$ atm. The Fe/SiO_2 ratio decreased as the oxygen partial pressure increased, which can be explained by the increasing concentration of iron deporting to the spinel. However, at oxygen partial pressure 10^{-11} atm, the ratio also reached a lower value in comparison to $p(O_2) = 10^{-10}$ atm. This can be explained by higher solubility of iron in the copper alloy in the most reducing conditions investigated, as shown in Fig. 3b.

The concentration of chemically dissolved copper in slag at iron-alumina spinel and copper saturation increased with

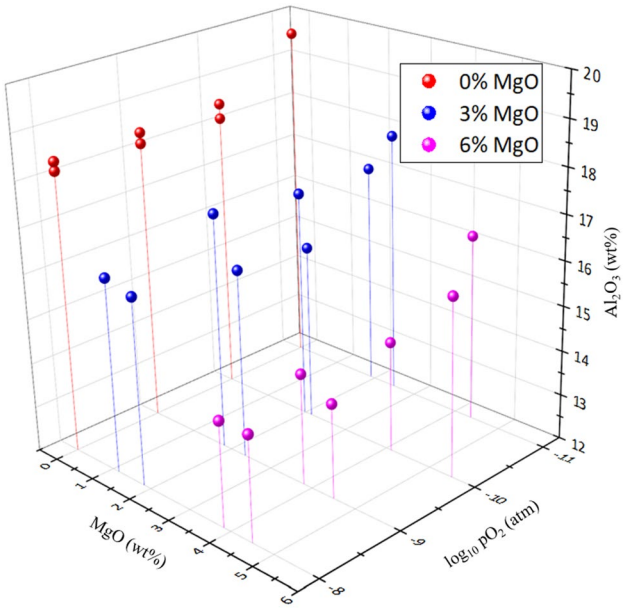

Fig. 5 Effect of MgO addition on alumina concentration in slag in oxygen partial pressure range from 10^{-11} to 10^{-8} atm

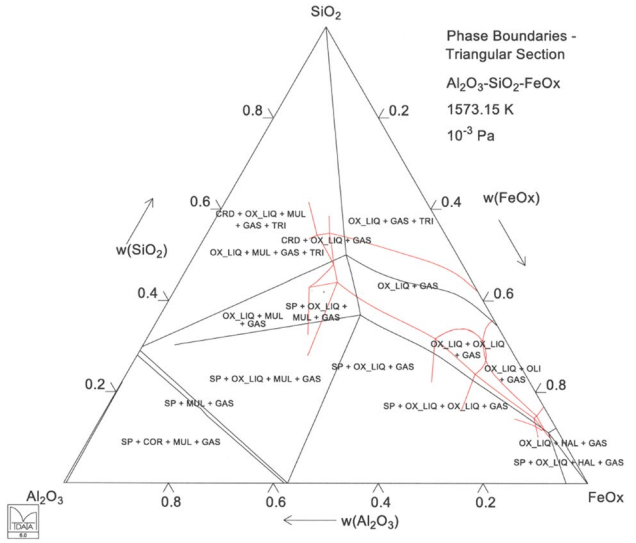

Fig. 6 Triangular section of Al_2O_3–SiO_2–FeO_x ternary system at $pO_2 = 10^{-8}$ atm. The phase boundaries with 0 (black lines) and 5 wt% MgO (red lines) have been superimposed. *OX_LIQ* slag, *SP* spinel, *TRI* tridymite, *MUL* mullite, *HAL* halite, *CRD* cordierite (Color figure online)

increasing oxygen partial pressure, as shown in Fig. 4b. The Cu concentration in slag increased strongly when $p(O_2)$ increased up to 10^{-8} atm, which is in fair agreement with the study of Nagamori et al. [34]. In their study, the copper solubility in slag was investigated in oxygen partial pressure range 10^{-8} to 10^{-9} atm, with higher Fe/SiO_2 ratios and alumina concentrations in slag. Our results are also in excellent agreement with the results of Klemettinen et al. [22] for copper solubility in alumina-iron spinel-saturated CaO-free and CaO-containing slags. The equilibrium concentration of copper at 1300 °C in $p(O_2) = 10^{-8}$ atm was approximately 2.4 wt% and under the most reducing conditions at $p(O_2) = 10^{-11}$ atm, it was approximately 0.25 wt%. Experiments with 3–6 wt% MgO addition studied in this work slightly reduced the copper solubility in the slags.

The concentrations of nickel and tin in the slags are presented in Fig. 4c and d. LA-ICP-MS results were utilized for nickel concentrations in the slags in all experimental conditions, and for tin concentrations in slags at oxygen partial pressures below 10^{-9} atm. As the oxygen partial pressure increased, the concentrations of both nickel and tin increased drastically, corresponding to the observations of Klemettinen et al. [29]. Magnesium oxide addition seemed to have only a slight effect on tin concentrations in the most oxidizing conditions of this study, where it decreased the deportment of tin in the slag.

The starting slag mixtures contained 0, 3, or 6 wt% MgO. At equilibrium, approximately 2/3 of MgO deported in the liquid slag and the remaining MgO in the solid spinel. The effect of MgO on the Al_2O_3 concentration in the slags is presented in Fig. 5. The Al_2O_3 concentration in the MgO-free slag varied between 18 and 20 wt%, depending on the oxygen partial pressure. Alumina concentration in the slag decreased significantly when the MgO concentration increased. When MgO concentration in slag reached approximately 4 wt%, the corresponding alumina concentration was between 14 and 16 wt%, increasing slightly towards the more reducing conditions. Therefore, the experimental results in this work are not only presented as a function of increasing magnesia, but also decreasing alumina concentration.

Figure 6 shows a triangular section of the FeO_x–SiO_2–Al_2O_3 phase diagram (black lines), with the influence of 5 wt% MgO addition (red lines) superimposed on the diagram. MTDATA software and the MTOX database [35] were employed for the calculations. According to the database, the addition of MgO results in the formation of new phases with relatively narrow stability regions. It also moves the spinel–mullite double saturation point towards the silica-rich corner, but the equilibrium alumina concentration in the liquid slag remains relatively constant. This does not correspond to our experimental observations; the addition of magnesia clearly decreased the equilibrium concentration of alumina in the slag.

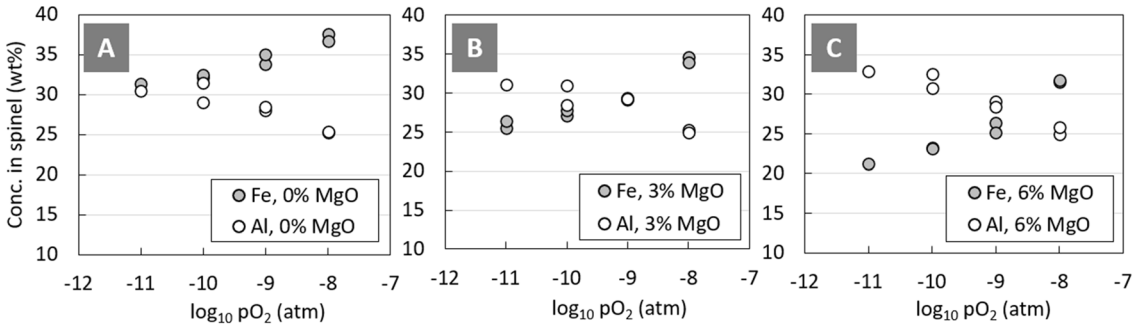

Fig. 7 The effect of magnesia on the equilibrium concentrations of iron and aluminum in the spinel phase

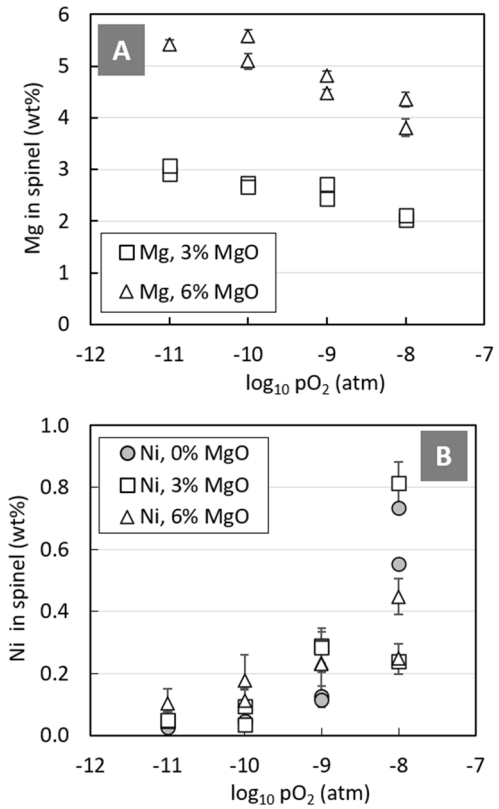

Fig. 8 Concentrations of magnesium and nickel in spinel as a function of oxygen partial pressure at 1300 °C

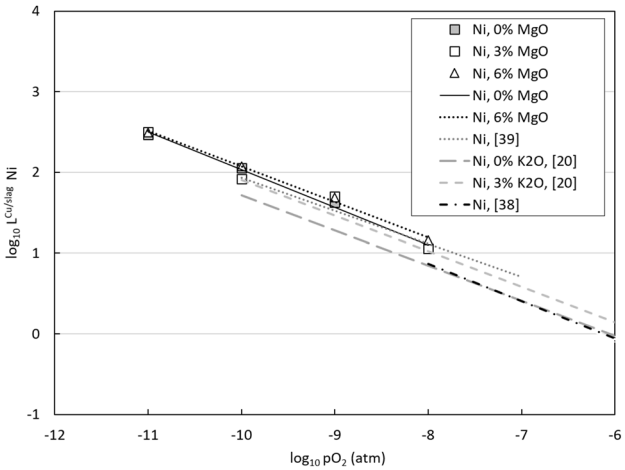

Fig. 9 The distribution coefficient of nickel between copper alloy and molten slag at 1300 °C for experimental data from this study (symbols and two trend lines) and from the literature, see the legend

Spinel

Figure 7 shows the aluminum and iron concentrations in discrete spinels as a function of oxygen partial pressure. The observed trends were similar for both MgO-free and MgO-bearing slags. Iron concentration in spinel increased as the $p(O_2)$ increased, whereas alumina concentration decreased. In the MgO-free system, the iron concentration in spinel was higher than aluminum concentration at $p(O_2) = 10^{-10}$–10^{-8} atm and reached approximately the same value at $p(O_2) = 10^{-11}$ atm, supporting the findings of Avarmaa et al. [27]. As magnesium deported into the spinel (Fig. 8a), it replaced a significant part of the divalent iron, therefore changing the composition of the spinel from iron-rich to alumina-rich below $p(O_2) = 10^{-9}$ atm.

The chemical composition of the spinels was not investigated with LA-ICP-MS technique because of the small size of the individual crystals. The concentration of nickel in the spinel, presented in Fig. 8b, was above the detection limits of EPMA. The concentration increased with increasing oxygen partial pressure, which is in good agreement with the earlier study of Klemettinen et al. [20]. The concentrations of tin in iron-alumina spinel were mostly below the detection limits of EPMA (supplementary Table S-3).

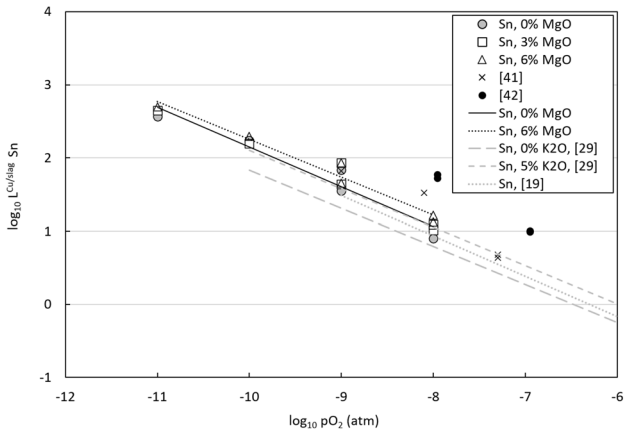

Fig. 10 The distribution coefficient of tin between copper alloy and molten slag at 1300 °C for experimental data from this study (symbols and two trend lines) and from the literature, see the legend

Distributions of Nickel and Tin

In equilibrium, the distribution of a metal [Me] between metal alloy and a molten oxide slag can be formulated as a chemical reaction (1):

$$[\mathrm{Me}] + \frac{\nu}{2}\mathrm{O}_2 = \left(\mathrm{MeO}_\nu\right), \tag{1}$$

where the symbols of [] and () brackets represent the alloy and slag phases, respectively; ν is a stoichiometric coefficient directly related with the oxidation degree of metal in the slag phase. The oxidation degree of metal in the liquid slag can be determined from the experimental distribution coefficient [36], which is a thermodynamic parameter that emphasizes how the element is partitioned between two phases in the investigated system. The distribution coefficient of a metal between metal alloy and liquid slag can be obtained from the following expression [37]:

$$\begin{aligned}\log_{10} L_{\mathrm{Me}}^{\mathrm{Cu/s}} &= \log_{10}\frac{[\mathrm{wt\%\ \ Me}]}{(\mathrm{wt\%\ \ Me})} \\ &= \log_{10}\frac{\left(f_{\mathrm{MeO}_\nu}\right)[n_{\mathrm{T}}]}{K[f_{\mathrm{Me}}](n_{\mathrm{T}})} - \frac{\nu}{2}\cdot\log_{10}p\left(\mathrm{O}_2\right) \\ &= \mathrm{A} - \nu/2\cdot\log_{10}p(\mathrm{O}_2),\end{aligned} \tag{2}$$

where $L_{\mathrm{Me}}^{\mathrm{Cu/s}}$ is the distribution coefficient of metal between copper alloy ('Cu') and slag ('s'), f denotes the Raoultian activity coefficients of Me and MeO_ν, and n_{T} corresponds to the total number of moles of constituents in 100 g of alloy and slag. The symbol A, which includes the thermodynamic equilibrium constant (K), is a constant in isothermal conditions [37, 38].

The distribution coefficients of nickel and tin, calculated from the experimental data, are shown in Fig. 9 and 10, respectively. Nickel and tin behave very similarly in the investigated system. The distributions of both metals favor the copper alloy at oxygen partial pressures below $p(\mathrm{O}_2) = 10^{-8}$ atm and the highest distribution coefficients were obtained in the most reductive conditions of oxygen partial pressure $p(\mathrm{O}_2) = 10^{-11}$ atm.

In Fig. 9, trend lines were fitted to the experimental points of the distribution coefficient of nickel. The average value of three slopes (for MgO-free and MgO-bearing slags) was around − 0.44. This indicates that nickel dissolves in the slag as NiO, which corresponds well with the study of Wang et al. [39] for iron silicate slag ($\mathrm{FeO_x}$–$\mathrm{SiO_2}$), even though in that study the concentration of nickel in metal alloy was much higher (approximately 9 wt%). Our results are also in very good agreement with the study of Klemettinen et al. [20] for $\mathrm{FeO_x}$–$\mathrm{SiO_2}$–$\mathrm{Al_2O_3}$ and $\mathrm{FeO_x}$–$\mathrm{SiO_2}$–$\mathrm{Al_2O_3}$–$\mathrm{K_2O}$ slags and of Sukhomlinov et al. [38] for pure, silica-saturated iron silicate slag ($\mathrm{FeO_x}$–$\mathrm{SiO_2}$). However, Klemettinen et al. [20] observed that the addition of $\mathrm{K_2O}$ in the slag increased the nickel distribution coefficient between metal alloy and slag. It was expected that the MgO addition in the slag would have a similar influence on the behavior of nickel, as it increases the slag basicity. However, based on our experimental data, MgO addition did not seem to have an obvious effect on the nickel distribution coefficient.

Figure 10 presents the distribution coefficient of tin between copper alloy and the slag. As discussed by Anindya et al. [40], some earlier studies presented that in reducing conditions of $p(\mathrm{O}_2)$ below 10^{-8} atm, tin exists predominantly as SnO and as $\mathrm{SnO_2}$ in more oxidizing conditions. In Fig. 10, the slopes of the trend lines fitted to the experimental points varied between 0.52 and 0.54, which suggests the dissolution of tin in the slag as divalent SnO. These trend line slopes are in good agreement with those calculated from previous studies where the tin concentrations were lower [19, 29]. The behavior of tin seems to be similar regardless of its starting concentration in the copper alloy (5 wt% in this study, 1 wt% in the previous studies [19, 29]).

Contrary to nickel distribution coefficient, the experimental results show that MgO addition has an increasing impact on the tin distribution coefficient between copper alloy and the slag. This observation is in agreement with the studies of Anindya et al. [40] and Klemettinen et al. [29], where higher concentrations of CaO and $\mathrm{K_2O}$ in the slag increased the tin distribution coefficient between metal alloy and slag. However, while comparing the results of our study with the study of Klemettinen et al. [29], it can be observed that the effect of MgO on tin distribution coefficient is smaller than that of $\mathrm{K_2O}$. This can be explained by the higher basicity of

K_2O and the less prominent effect of K_2O on the equilibrium solubility of Al_2O_3 in the slag.

The earlier experimental data from See and Rankin [41] are in good agreement with our results, but the values obtained by Anindya et al. [42] using olivine slags are somewhat higher. A comparison of our results with the results obtained by Klemettinen et al. [29], Avarmaa et al. [19], and Sukhomlinov et al. [38] using FeO_x–SiO_2–Al_2O_3, FeO_x–SiO_2–Al_2O_3(–K_2O), and FeO_x–SiO_2 slags, respectively, suggests that saturating the slag with alumina does not have a significant impact on the distribution behavior of nickel and tin. Klemettinen et al. [20, 29] indicated that K_2O addition has definitively an increasing effect on the nickel and tin distribution coefficients. In our study, the MgO addition only had a slight increasing effect for tin, and no clear effect was observed for nickel. However, as presented in Fig. 5, the effect of MgO alone could not be isolated in the results, due to the decreasing Al_2O_3 concentration in the slag with increasing MgO concentration. Therefore, some additional calculations were performed based on dilute solution theory.

In a system where one substance is solvent and there are several solutes, the activity coefficients of the various solutes affect the activity coefficient of the metal. Wagner proposed [43] an Eq. (3), which presents an expansion of the logarithm of the activity coefficient of a solute as a linear function of the concentrations of the other solutes:

$$\log_{10} f_i\left(x_1, x_2, x_3, \ldots\right) = \log_{10} f_i^0 + x_1\varepsilon_1^i + x_2\varepsilon_2^i + x_3\varepsilon_3^i + \cdots, \quad (3)$$

where f_i is activity coefficient; f_i^0 activity coefficient of the metal in infinite dilution; x_1, x_2, x_n are mole fractions of solutes; and $\varepsilon_1{}^i$, $\varepsilon_2{}^i$, $\varepsilon_3{}^i$ are the first-order interaction coefficients.

Table 2 Calculated values for interaction coefficients and their standard errors

	Value	Standard error
$C_{(Ni)}$	− 3.0046	0.0512
$\varepsilon^{NiO}_{Al_2O_3}$	0.0027	0.0037
ε^{NiO}_{MgO}	0.0053	0.0165
$C_{(Sn)}$	− 3.1715	0.9134
$\varepsilon^{SnO}_{Al_2O_3}$	0.0148	0.0495
ε^{SnO}_{MgO}	0.0488	0.0483

In the case of our study, the effect of MgO and Al_2O_3 interactions with metal oxide MeO_x was investigated. The expression was limited to first-order interaction parameters and for simplifying the approach, the SiO_2 and FeO_x interactions were excluded from the calculations. The following Equation was proposed:

$$\log_{10} f_{MeO_x} = \log_{10} f^0_{MeO_x} + \varepsilon^{MeO_x}_{MgO} \cdot x_{MgO} + \varepsilon^{MeO_x}_{Al_2O_3} \cdot x_{Al_2O_3} \quad (4)$$

After combining above Eq. (4) with the equation describing the distribution coefficient of the metal between metal alloy and liquid slag, the following Eqs. (5 and 6) were obtained:

$$\log_{10} L^{Cu/s}_{Me} = C - \nu/2 \cdot \log_{10} p(O_2) + \varepsilon^{MeO_x}_{MgO} \cdot x_{MgO} + \varepsilon^{MeO_x}_{Al_2O_3} \cdot x_{Al_2O_3} \quad (5)$$

$$\log_{10} L^{Cu/s}_{Me} + \nu/2 \cdot \log_{10} p(O_2) = C + \varepsilon^{MeO_x}_{MgO} \cdot x_{MgO} + \varepsilon^{MeO_x}_{Al_2O_3} \cdot x_{Al_2O_3} \quad (6)$$

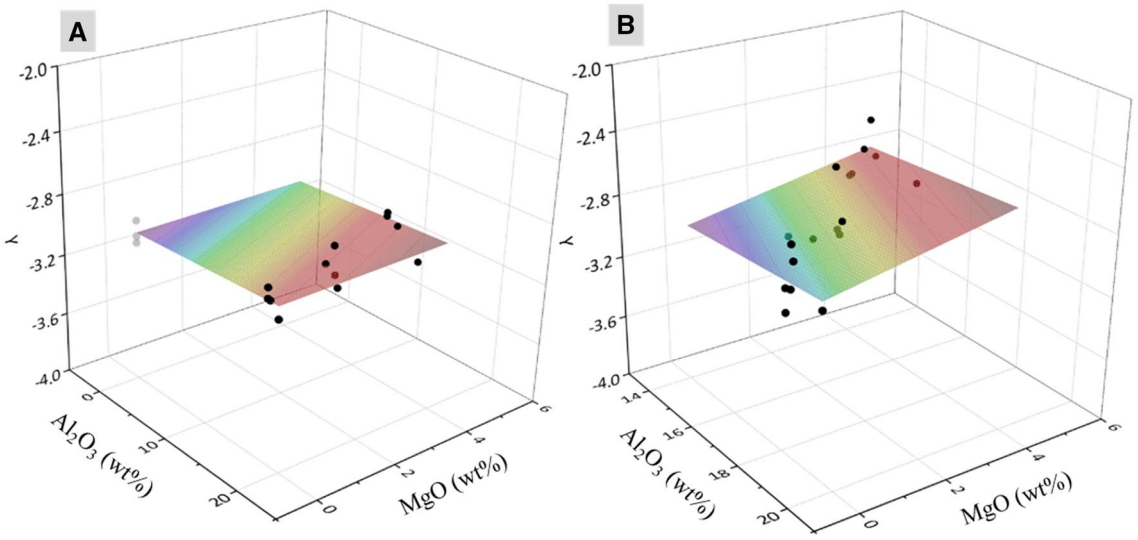

Fig. 11 Plotting the left side of Eq. 6 (symbol *Y*) as a function of MgO and Al_2O_3 concentrations in slags for nickel (**a**) and tin (**b**). Gray points in Ni graph represent data from the study of Sukhomlinov et al. [38] for FeO_x–SiO_2 system without MgO and Al_2O_3 additions

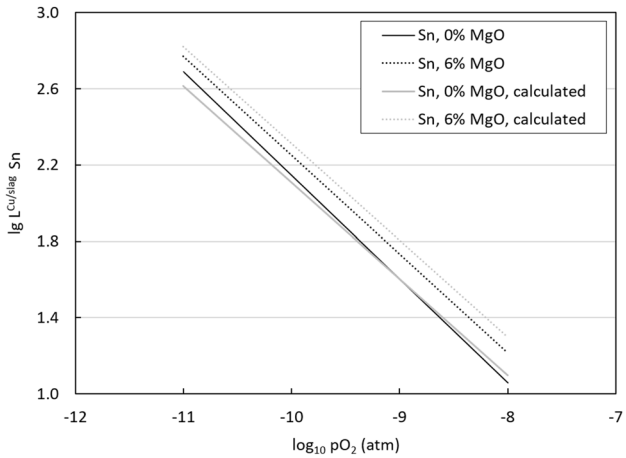

Fig. 12 Distribution coefficient of tin between copper alloy and slags. The black trend lines were fitted based on experimental data, whereas the gray trend lines were refined based on the recalculations. The oxide form SnO (corresponding to a slope of − 0.5) was used for the calculations, whereas the slope from the experimental data was between − 0.52 and − 0.54

The left side of the above Eq. (6) was plotted as a function of MgO and Al_2O_3 concentrations in the slag (experimental data), and a plane was fitted to the datapoints in Origin software (OriginPro 2020). For nickel, the results from the study of Sukhomlinov et al. [38] for the FeO_x–SiO_2 system were added, so that results without Al_2O_3 in the slag could also be included in the fitting. Naturally, as the experimental set-up was not identical to our study, the data were not a perfect match. The results for plotting the left side of Eq. (6) as a function of MgO and Al_2O_3 concentrations, as well as the fitted planes, are shown in Fig. 11 for nickel (a) and tin (b). The values obtained for Al_2O_3 and MgO interaction coefficients, presented in Table 2, are positive, which suggests that the increasing concentrations of these oxides enhance the deportments of nickel and tin into the metal alloy.

The interaction coefficient values are higher for tin than for nickel, indicating that MgO and Al_2O_3 have a more prominent effect on the distribution behavior of tin. The standard errors are similar or even higher than the actual values, and therefore these calculations should be regarded only as directional, not absolute. For nickel, the amount of datapoints included in the fitting from this study was lower than for tin, because the slag concentration results from LA-ICP-MS were used, and only one experimental series was analyzed with that method.

For testing the interaction coefficient values obtained, the distribution coefficients were recalculated with Eq. (4) so that the alumina concentration in the slag remained constant, and only the magnesia concentration increased. This means that the Al_2O_3 concentration values from the slag without MgO, analyzed with EPMA, were used for the other slags with the actual MgO concentration values (from EPMA). Figure 12 shows the experimentally obtained and recalculated trend lines for tin distribution coefficients between copper alloy and the slag as a function of oxygen partial pressure. It can be observed that according to the recalculated results, when the alumina concentration remains constant, the effect of MgO addition becomes clearer, as expected. Similar recalculations for nickel (not presented here) did not indicate a refined effect on the distribution coefficient, which is most likely due to the smaller amount of experimental data available for the fitting.

Conclusions

Although some experimental work has been done on the effects of CaO, Al_2O_3, and K_2O on slag chemistry and trace element distribution experiments in secondary copper smelting have been performed, data on the effect of MgO addition to slag chemistry in secondary copper smelting are still limited in the literature. Therefore, one goal of this study was to analyze the impact of MgO addition on the phase equilibria of high-alumina iron silicate slags. In the investigated system, alumina concentration in slag at spinel saturation decreased with increasing magnesia concentration and therefore, the effect of MgO alone could not be isolated. This 4D effect was not evident in the phase diagram calculations performed with MTOX database of MTDATA software. The results indicated that the MgO addition increased the number of spinel grains (discrete spinels) observed in the slag and had a significant impact on spinel composition. As magnesium deported into the spinel, it replaced a significant part of the divalent iron, therefore changing the compositions of the spinel, which converted from iron-rich to alumina-rich below $p(O_2) = 10^{-9}$ atm.

The distribution coefficients obtained for nickel and tin between copper alloy and the slags are in good agreement with the data obtained in previous studies for high-alumina iron silicate slags and alumina-free slags. Our experimental results showed that MgO addition has an increasing effect on the distribution coefficient of tin, whereas no clear effect was observed for nickel. Theoretical calculations based on the equation proposed by Wagner dilute solution model [43] confirmed the effect for tin.

Based on the results of this work, low concentrations of MgO (up to 6 wt%) had a positive effect on the recoveries of copper and tin in the metal alloy, and no effect on the recovery of nickel. However, as the MgO addition may cause increasing formation of suspended solids in the slag, viscosity of the slag may increase, which has a negative impact on an industrial operation of a smelter.

Acknowledgements The experimental work was conducted in the Business Finland funded SYMMET project (Project No.

3891/31/2018). L.K. is grateful for the Finnish Steel and Metal Producer's Fund for a doctoral study grant. Mr. Lassi Pakkanen at Geological Survey of Finland is highly acknowledged for his work regarding the EPMA analyses. The Academy of Finland's RAMI infrastructure based jointly at Aalto University, GTK Espoo and VTT Espoo, was utilized in this work.

Funding Open access funding provided by Aalto University.

Compliance with Ethical Standards

Conflict of interest The authors declared that they have no conflict of interest.

References

1. Baldé CP, Forti V, Gray V, Kuehr R, Stegmann P (2017) The Global E-waste Monitor 2017, United Nations University (UNU), International Telecommunication Union (ITU) and International Solid Waste Association (ISWA), Bonn. https://collections.unu.edu/eserv/UNU:6341/Global-E-waste_Monitor_2017_electronic_single_pages_pdf. Accessed 8 April 2020
2. Ongondo FO, Williams ID, Cherrett TJ (2011) How are WEEE doing? A global review of the management of electrical and electronic wastes. Waste Manag 31:714–730. https://doi.org/10.1016/j.wasman.2010.10.023
3. Charles RG, Douglas P, Dowling M, Liversage G, Davies ML (2020) Towards increased recovery of critical raw materials from WEEE—evaluation of CRMs at a component level and pre-processing methods for interface optimisation with recovery processes. Resour Conserv Recycl. https://doi.org/10.1016/j.resconrec.2020.104923
4. Ghodrat M, Rhamdhani MA, Brooks G, Rashidi M, Samali B (2017) A thermodynamic-based life cycle assessment of precious metal recycling out of waste printed circuit board through secondary copper smelting. Environ Dev 24:36–49. https://doi.org/10.1016/j.envdev.2017.07.001
5. Cui J, Zhang L (2008) Metallurgical recovery of metals from electronic waste: A review. J Hazard Mater 158:228–256. https://doi.org/10.1016/j.jhazmat.2008.02.001
6. Ebin B, Isik MI (2016) Pyrometallurgical processes for the recovery of metals from WEEE. In: WEEE recycling—research, development, and policies. Elsevier, Amsterdam, pp 107–137. https://doi.org/10.1016/B978-0-12-803363-0.00005-5
7. Ghodrat M, Rhamdhani MA, Brooks G, Masood S, Corder G (2016) Techno economic analysis of electronic waste processing through black copper smelting route. J Clean Prod 126:178–190. https://doi.org/10.1016/j.jclepro.2016.03.033
8. Shuva MAH, Rhamdhani MA, Brooks GA, Masood S, Reuter MA (2016) Thermodynamics data of valuable elements relevant to e-waste processing through primary and secondary copper production: a review. J Clean Prod 131:795–809. https://doi.org/10.1016/j.jclepro.2016.04.061
9. Götze R, Rotter VS (2012) Challenges for the recovery of critical metals from waste electronic equipment—a case study of indium in LCD panels. In: Electronics Goes Green 2012+ (EGG). IEEE, pp 1–8
10. Kim HG, Sohn HY (1998) Effects of CaO, Al_2O_3, and MgO additions on the copper solubility, ferric/ferrous ratio, and minor-element behavior of iron-silicate slags. Metall Mater Trans B 29:583–590
11. Khaliq A, Rhamdhani MA, Brooks G, Masood S (2014) Metal extraction processes for electronic waste and existing industrial routes: a review and Australian perspective. Resources 3:152–179. https://doi.org/10.3390/resources3010152
12. Jiang T, Wang S, Guo Y, Chen F, Zheng F (2016) Effects of basicity and MgO in slag on the behaviors of smelting vanadium titanomagnetite in the direct reduction-Electric furnace process. Metals 6:107. https://doi.org/10.3390/met6050107
13. Kowalczyk J, Mroz W, Warczok A, Utigard TA (1995) Viscosity of copper slags from chalcocite concentrate smelting. Metall Mater Trans B 26(1):1217–1223
14. Elliot BJ, See JB, Rankin WJ (1978) Effects of slag composition on copper losses to silica saturated iron silicate slags. Trans Met Min Met 87:C204–C211
15. Degterov SA, Pelton AD (1999) A thermodynamic database for copper smelting and converting. Metall Trans B 30(4):661–669. https://doi.org/10.1007/s11663-999-0027-4
16. Henao HM, Nexhip C, George-Kennedy DP, Hayes PC, Jak E (2010) Investigation of liquidus temperatures and phase equilibria of copper smelting slags in the FeO-Fe_2O_3-SiO_2-CaO-MgO-Al_2O_3 system at PO_2 10^{-8} atm. Metall Mater Trans B 41:767–779. https://doi.org/10.1007/s11663-010-9369-1
17. Henao HM, Pizarro C, Font J, Moyano A, Hayes PC, Jak E (2010) Phase equilibria of "Cu_2O"-"FeO"–CaO–MgO–Al_2O_3 slags at PO_2 of 10–8.5 atm in equilibrium with metallic copper for a copper slag cleaning production. Metall Mater Trans B 41:1186–1193. https://doi.org/10.1007/s11663-010-9434-9
18. Hasan MM, Rhamdhani MA, Shuva MAH, Brooks GA (2020) Study of the structure of FeO_x–CaO–SiO_2–MgO and FeO_x–CaO–SiO_2–MgO-Cu_2O-PdO slags relevant to urban ores processing through Cu smelting. Metals 10(1):78. https://doi.org/10.3390/met10010078
19. Avarmaa K, Klemettinen L, O'Brien H, Taskinen P (2019) The behavior of tin in black copper smelting conditions with different iron-silicate based slags. In: Proceedings of EMC 2019, vol 2. GDMB Verlag GmbH, Clausthal-Zellerfeld, pp 497–510
20. Klemettinen L, Avarmaa K, O'Brien H, Taskinen P, Jokilaakso A (2018) Behavior of nickel as a trace element and time-dependent formation of spinels in WEEE smelting. In: Extraction 2018, The Minerals, Metals & Materials Series, pp 1073–1082
21. Dańczak A, Klemettinen L, Kurhila M, Taskinen P, Lindberg D, Jokilaakso A (2020) Behavior of battery metals lithium, cobalt, manganese and lanthanum in black copper smelting. Batteries 6(1):16. https://doi.org/10.3390/batteries6010016
22. Klemettinen L, Avarmaa K, Taskinen P (2017) Slag chemistry of high-alumina iron silicate slags at 1300 degrees C in WEEE smelting. J Sustain Met 3(4):772–781. https://doi.org/10.1007/s40831-017-0141-5
23. Davies RH, Dinsdale AT, Gisby JA, Robinson JAJ, Martin SM (2002) MTDATA—thermodynamics and phase equilibrium software from the National Physical Laboratory. CALPHAD 26(2):229–271. https://doi.org/10.1016/S0364-5916(02)00036-6

24. Bastin GF, Heijligers HJM (1990) Quantitative electron probe microanalysis of ultralight elements (boron-oxygen). Scanning 12:225–236. https://doi.org/10.1002/sca.4950120408
25. van Achterberg E, Ryan C, Jackson S, Griffin W (2001) Laser ablation ICP-MS in the Earth Science. Mineralogical Association of Canada, Short Course Series #29, St John, pp 239–243
26. Jochum KP, Weis U, Stoll B, Kuzmin D, Yang Q, Raczek I, Jacob DE, Stracke A, Birbaum K, Frick DA, Günther D, Enzweiler J (2011) Determination of reference values for NIST SRM 610–617 glasses following ISO guidelines. Geostand Geoanal Res 35(4):397–429. https://doi.org/10.1111/j.1751-908X.2011.00120.x
27. Avarmaa K, Yliaho S, Taskinen P (2018) Recoveries of rare elements Ga, Ge, In and Sn from waste electric and electronic equipment through secondary copper smelting. Waste Manag 71:400–410. https://doi.org/10.1016/j.wasman.2017.09.037
28. De Wilde E, Bellemans I, Campforts M, Khaliq A, Vanmeensel K, Seveno D, Guo M, Rhamdhani MA, Brooks G, Blanpain B, Moelans N, Verbeken K (2015) (2015) Wetting behaviour of Cu based alloys on spinel substrates in pyrometallurgical context. Mater Sci Technol 31(15):1925–1933. https://doi.org/10.1179/1743284715Y.0000000052
29. Klemettinen L, Avarmaa K, O'Brien H, Taskinen P, Jokilaakso A (2019) Behavior of tin and antimony in secondary copper smelting process. Minerals 9(1):39. https://doi.org/10.3390/min9010039
30. Avarmaa K, O'Brien H, Klemettinen L, Taskinen P (2019) Precious metal recoveries in secondary copper smelting with high-alumina slags. J Mater Cycles Waste Manag 22:642–655. https://doi.org/10.1007/s10163-019-00955-w
31. De Wilde E, Bellemans I, Kampforts M, Guo M, Blanpain B, Moelans N, Verbeken K (2016) Investigation of high temperature slag/copper/spinel interactions. Metall Mater Trans B 47:1–14. https://doi.org/10.1007/s11663-016-0805-8
32. De Wilde E, Bellemans I, Kampforts M, Guo M, Vanmeensel K, Blanpain B, Moelans N, Verbeken K (2017) Study of the effect of spinel composition on metallic copper losses in slags. J Sustain Metall 3:416–427. https://doi.org/10.1007/s40831-016-0106-0
33. Bellemans I, De Wilde E, Blanpain B, Moelans N, Verbeken K (2017) Investigation of origin of attached Cu-Ag-droplets to solid particles during high temperature slag/copper/spinel interactions. Metall Mater Trans B 48(6):3058–3073
34. Nagamori M, Mackey PJ, Tarassoff P (1975) Copper solubility in FeO-Fe_2O_3-SiO_2-Al_2O_3 slag and distribution equilibria of Pb, Bi, Sb and As between slag and metallic copper. Metall Mater Trans B 6(2):295–301
35. Gisby J, Taskinen P, Pihlasalo J, Li Z, Tyrer M, Pearce J, Avarmaa K, Bjorklund P, Davis H, Korpi M, Martin S, Personen L, Robinson JA (2017) MTDATA and the prediction of phase equilibria in oxide systems: 30 years of industrial collaboration. Metall Mater Trans B 48(1):91–98. https://doi.org/10.1007/s11663-016-0811-x
36. IUPAC (1997) Compendium of chemical terminology, 2nd edn (the "Gold Book"). Compiled by McNaught AD, Wilkinson A, Blackwell, Oxford. Online version (2019–) created by Chalk SJ. ISBN 0-9678550-9-8. https://doi.org/10.1351/goldbook. Accessed 8 April 2020
37. Takeda Y, Ishiwata S, Yazawa A (1983) Distribution equilibria of minor elements between liquid copper and calcium ferrite slag. Trans Jpn Inst Met 24:518–528
38. Sukhomlinov D, Klemettinen L, Avarmaa K, O'Brien H, Taskinen P, Jokilaakso A (2019) Distribution of Ni Co, precious, and platinum group metals in copper making process. Metall Mater Trans B 50(4):1752–1765. https://doi.org/10.1007/s11663-019-01576-2
39. Wang SS, Kurtis AJ, Toguri JM (1973) Distribution of copper-nickel and copper-cobalt between copper-nickel and copper-cobalt alloys and silica saturated fayalite slags. Can Metall Q 12(4):383–390
40. Anindya A, Swinbourne DR, Reuter MA, Matusewicz RW (2013) Distribution of elements between copper and FeO_x-CaO-SiO_2 slags during pyrometallurgical processing of WEEE Part 1—tin. Min Proc Ext Met 122(3):165–173
41. See JB, Rankin WJ (1981) Copper losses and the distribution of impurities in the systems FeO-Fe_2O_3-SiO_2-Al_2O_3-Cu and FeO-Fe_2O_3-SiO_2-Al_2O_3-CaO-Cu at 1300 °C. National Institute for Metallurgy, Process Development Division, Report No. 2099, South Africa
42. Anindya A, Swinbourne D, Reuter M, Matusewicz R (2009) Tin distribution during smelting of WEEE with copper scrap. In: Proceedings of EMC 2009, GDM (Goslar), Innsbruck, Austria, pp 555–567
43. Wagner C (1952) Equations of state for solutions with substantially disordered atomic distribution. In: Thermodynamics and alloys. Addison-Wesley, Cambridge, pp 31–53